Journal of Luminescence 258 (2023) 119812

Contents lists available at ScienceDirect

Journal of Luminescence

journal homepage: www.elsevier.com/locate/jlumin

Full Length Article

Narrow-linewidth external cavity semiconductor laser based on permanent index modulated grating optical feedback for radiation resistance

Jia-Qi Chen [a,b], Chao Chen [a,b,c,*], Qi Guo [d], Li Qin [a,c], Jian-Wei Zhang [a], Hang-Yu Peng [a,**], Jing-Jing Sun [a], Xing Zhang [a], Hao Wu [a], Yin-Li Zhou [a], Yong-Sen Yu [d], Yong-Qiang Ning [a,c], Li-Jun Wang [a]

[a] State Key Laboratory of Luminescence and Application, Changchun Institute of Optics, Fine Mechanics and Physics, Chinese Academy of Sciences, Changchun, 130033, China
[b] Center of Materials Science and Optoelectronics Engineering, University of Chinese Academy of Sciences, Beijing, 100049, China
[c] Xiongan Innovation Institute, Chinese Academy of Sciences, Xiongan, 071800, China
[d] State Key Laboratory of Integrated Optoelectronics, College of Electronic Science and Engineering, Jilin University, Changchun, 130012, China

ARTICLE INFO

Keywords:
Semiconductor laser
Narrow linewidth, radiation resistance
Apodized fiber grating, permanent index modulated

ABSTRACT

We demonstrate a narrow-linewidth external cavity semiconductor laser (ECSL) based on permanent index modulated Bragg grating feedback for radiation resistance. The frequency selection device of the laser is a highly stable fiber Bragg grating (FBG) created with a femtosecond laser. The laser shows excellent radiation resistance after passing through radiation, which is assessed with a γ-ray total ionizing dose (TID) radiation test. The Lorentz linewidth and relative intensity noise (RIN) of the laser show almost no change after irradiation, and are less than 15 kHz and −150 dBc/Hz, respectively. The maximum output power and laser wavelength slightly change after irradiation increasing by 3.79% and redshifting by 9.10 p.m., respectively, compared with those before irradiation. The experimental results show that the compact-structure and low-cost semiconductor laser based on the permanent index modulated Bragg grating has outstanding stability and robustness against harsh-radiation environments, and it can meet the radiation resistance requirements of space laser communication applications for light sources.

1. Introduction

Charged particles in the space radiation environment will lead to abnormal operation or even failure of optoelectronic devices, which will greatly affect the reliability and life of spacecraft [1]. The radiation resistance of optoelectronic devices is improved by adding radiation shielding on their surfaces, but this often leads to extra mass. The weight requirement is very strict for aircraft, especially for spacecraft; thus, the radiation resistance of optoelectronic devices must be improved [2]. Narrow-linewidth semiconductor lasers are widely used in space laser communication [3,4], cold atom experiments [5,6], and gravitational wave detection [7,8] because of their compact structure, high reliability and high photoelectric efficiency. The stability of their spectrum, power, linewidth and other performance parameters in the space radiation environment as light source devices directly determines the stability and reliability of the above application systems [3–8]. Therefore, the radiation resistance of narrow-linewidth semiconductor lasers in the space radiation environment must be investigated.

Traditional external cavity semiconductor lasers (ECSLs), such as those using etalons, volume gratings and diffraction gratings, can exhibit significantly reduced linewidth, but their sensitivity to environmental vibration and low integration affect the reliability and stability of the lasers [9,10]. Although distributed Bragg reflection and distributed Bragg feedback lasers are compact in structure, they usually have short cavity lengths, which results in short photon lifetimes and limits the linewidth performance [11,12]. Integrated ECSLs based on fiber Bragg gratings (FBGs) have attracted attention due to their compact and stable cavity structure with extremely low intensity noise levels and narrow linewidths, and they also have the advantages of low cost and easy preparation [13–15]. FBGs have become a strong

* Corresponding author. State Key Laboratory of Luminescence and Application, Changchun Institute of Optics, Fine Mechanics and Physics, Chinese Academy of Sciences, Changchun, 130033, China.
** Corresponding author.
E-mail addresses: chenc@ciomp.ac.cn (C. Chen), penghy@ciomp.ac.cn (H.-Y. Peng).

https://doi.org/10.1016/j.jlumin.2023.119812
Received 6 February 2023; Received in revised form 3 March 2023; Accepted 15 March 2023
Available online 18 March 2023
0022-2313/© 2023 Elsevier B.V. All rights reserved.

competitor for space application lasers. Their adaptability to the space environment is not only affected by radiation-hardened packaging but also closely related to the radiation resistance of the fiber gratings, which depends on the formation mechanism of the gratings.

Presently, the preparation methods for the above grating mainly include ultraviolet excimer laser writing (UV-writing) technology and femtosecond laser writing (fs-writing) technology [16–20], and their grating formation mechanisms are essentially different. The UV-written FBG is based on the light-induced refractive index, and periodic refractive index modulation is achieved by trapping electrons or holes through defects to form "color centers". The color centers are easily erased under the irradiation of high-energy particles, which affects the radiation resistance of the grating [16,17]. The fs-writing technology for FBGs uses the peak power density of ultrashort pulses to induce breakage of chemical bonds in fiber materials to change the defect precursors and form permanent refractive index modulation. This effectively prevents the grating from being changed by γ-ray irradiation [18–20]. Existing research has confirmed that fs-written FBGs have radiation resistance that cannot be matched by UV-written FBGs. For example, A. Morana et al. demonstrated the X-ray radiation response of gratings written by different laser light sources and confirmed that the fs-written FBG has excellent radiation resistance using 1 MGy total radiation measurements [20].

In this work, we demonstrate a narrow-linewidth ECSL based on a fs-written permanent index modulated FBG. We apply γ-ray total ionizing dose (TID) irradiation to the laser. The laser shows excellent radiation resistance, and the performance changes very little after the TID test. The minimum Lorentz linewidth and relative intensity noise (RIN) are less than 15 kHz and −150 dBc/Hz, respectively, and they are relatively stable before and after irradiation. The change in photoelectric characteristics after irradiation is minimal. The maximum output power is only increased by 3.79% and the laser wavelength is redshifted by 9.10 p.m. compared with those before irradiation. The laser source proposed in this work reduces the need for antiradiation packaging, and the semiconductor laser with a narrow linewidth can not only be used in space laser communication due to its **c**ompact structure and low cost, but also be extended to gas sensing and precise measurement based on the laser spectrum [21–23].

2. Laser structure and irradiation experiment

2.1. Structure and fabrication

A schematic of the ECSL is shown in Fig. 1(a). The laser is composed of a semiconductor gain chip and a permanent index modulated Bragg grating, which are coupled and integrated through an aspheric lens. The narrow ridge quantum dot (QD) gain chip in the 1-μm band is used as the gain medium [24,25], and the chip cavity length (L_{GC}) is 1.50 mm. A significant advantage of the QD structure is the resilience of the photoluminescence and carrier lifetime in high-energy radiation environments due to the additional lateral isolation of injected carriers within the gain region, which show excellent radiation resistance in Ref. [26]. The chip is a narrow ridge curved waveguide structure (with an inclination angle of 7°). Both ends of the waveguide are coated with a 90% high-reflection coating (R_1) and a 0.01% antireflection coating to reduce the influence of the internal cavity mode on frequency selection. The black curve in Fig. 2 shows the amplified spontaneous emission spectrum of the gain chip under 100 mA, and the cavity surface resonance is effectively suppressed.

In addition, the FBG used to provide optical feedback is prepared in a

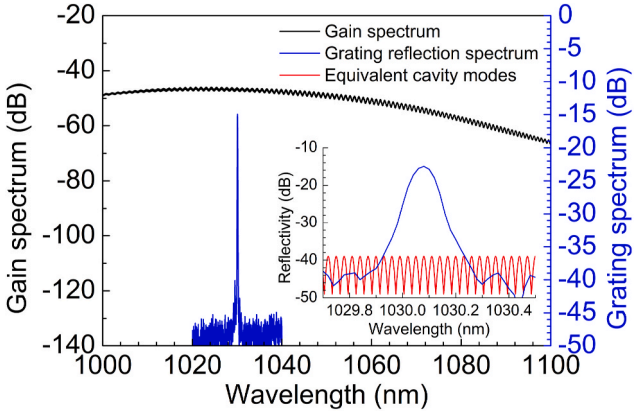

Fig. 2. Gain spectrum (black line) of the gain chip and reflection spectrum (blue line) of the FBG under 100 mA. The inset shows the frequency selection mechanism of the FBG and the mode distribution of the equivalent cavity (red line).

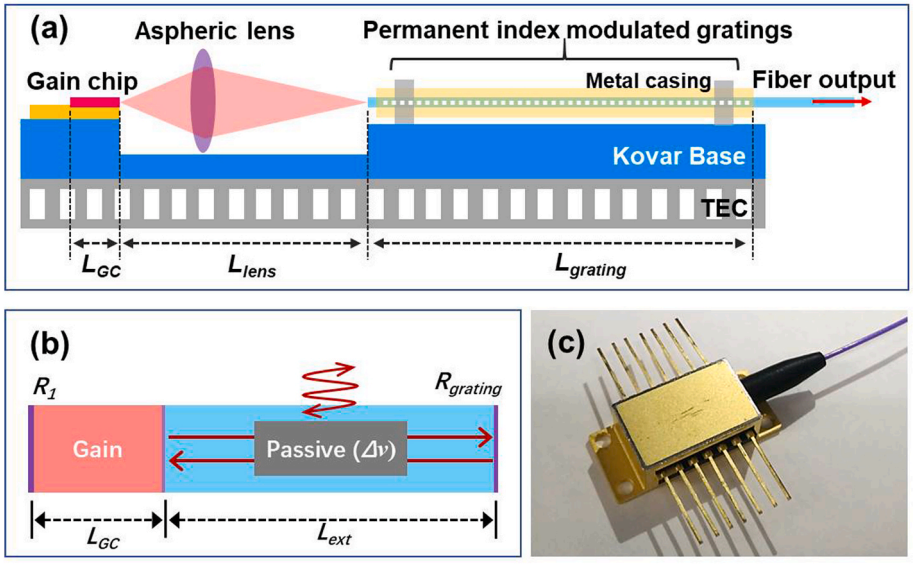

Fig. 1. (a) Schematic of the ECSL device for radiation resistance, (b) simple model of the laser structure, and (c) photograph of the laser.

single-mode fiber (Corning, HI 1060 fiber) by femtosecond laser point-by-point technology [27]. The femtosecond laser used has a wavelength of 515 nm and a pulse width of 290 fs. The apodization distribution of the grating must be modulated to achieve a laser output with a high sidemode suppression ratio (SMSR). Therefore, we use an apodized FBG instead of a uniform FBG to effectively suppress the sidelobe and improve the SMSR of the FBG spectrum through energy regulation. Specifically, the femtosecond pulse energy is controlled and adjusted to make the refractive index modulation amplitude conform to the apodization function distribution during the preparation process. The specific preparation method has been described in detail in Ref. [28]. The length ($L_{grating}$) of the prepared third-order femtosecond apodized FBG is 6.00 mm with a period of 1.064 μm and a wavelength of 1030 nm. The blue curve in Fig. 2 shows the reflection spectrum of the FBG. The full-width at half-maximum of the FBG reflection peak is measured to be 80.00 p.m. with an SMSR of 25.20 dB and a reflectivity ($R_{grating}$) of 24.62%. The low reflectivity can ensure high output power of the laser.

The semiconductor gain chip and fs-written FBG are coupled and integrated through an aspherical lens (with a total working length of 6.25 mm) to form an equivalent resonator structure, as shown in Fig. 1 (b), and they are packaged into a standard butterfly laser, as shown in Fig. 1 (c). The equivalent cavity of the laser can be considered a combination of an active gain region and a passive external cavity. The inset in Fig. 2 shows the equivalent cavity mode and the peak portion of the Bragg reflection spectrum. The equivalent cavity mode is locked at the peak wavelength of Bragg resonance. The Bragg band gap of the passive grating provides mode selection and optical feedback, and the return light passes through the gain chip to achieve gain amplification of the locked mode. The quality factor Q of the resonator is increased by expanding the cavity length of the resonator, and the photon life is extended; thus, the effective linewidth is narrowed. In addition, an increase in the output power is also helpful for achieving a narrower linewidth. This is also confirmed by the variation in the linewidth with current mentioned in Fig. 6 below. The equivalent cavity length (L_{ext}) of the laser is approximately 10.75 mm, which is composed of the gain chip length, the aspheric mirror working length and half of the FBG length, and the corresponding free spectral range (FSR) is 31.8 p.m. A single-frequency and narrow-linewidth laser output can be ensured based on the above mode selection, linewidth narrowing mechanism and consideration of the gain characteristics.

2.2. Irradiation experiment

Relevant research shows that the TID response characteristics of photoelectric devices in a certain range are related to the dose rate and the total radiation amount for space radiation experiments of optoelectronic devices such as lasers, but they are almost independent of the radiation type [29,30]. Therefore, radiation effect research in the laboratory generally uses only one radiation source to produce a dose rate and a total radiation amount approximately equivalent to those in the space environment. In this case, we use a γ-ray TID irradiation experiment for the laser [31]. The radionuclide Co^{60} after radioactive decay is selected as the steady-state γ-ray radiation source. The laser and the radiation source are placed in a thick-wall lead container during the test. When conducting offline radiation experiments, the laser is in the off state during irradiation. The irradiation experiment is conducted at room temperature with a dose rate of 50 rad/s, and the irradiation is completed when the dose accumulates to 100 krad.

3. Results and discussion

The key performance characteristics of lasers, such as the linewidth, phase noise and RIN, are not only limited by the inherent structure of the laser but also affected by the measurement accuracy and stability of the laser controller. To avoid such problems, an ultralow-noise current source (LDX-3620B, ILX Lightwave Corporation) and a thermoelectric temperature controller (TEC) (LDT-5910C, ILX Lightwave Corporation) are used to accurately and stably control the current and temperature of the laser during the test process. The laser is equipped with a low-pass filter (LNF-320, ILX Lightwave Corporation) to further suppress the injected current ripple noise. The above test devices can effectively avoid the introduction of technical noise. In addition, all tests of the laser are carried out at room temperature, and the TEC temperature is set at 25 °C.

3.1. Spectra and power–current–voltage characteristics

To systematically analyze the spectrum and power–current–voltage (P–I–V) characteristics of the laser before and after irradiation, the lasing spectra for different injection currents are measured in detail with a spectral analyzer (wavelength resolution set at 20 p.m.) (AQ6370B, Yokogawa), and the P–I–V characteristics are recorded using a power meter and a current source. The TEC temperature of the laser is set to 25 °C, and the injection current ranges from 0 mA to 400 mA in this process.

Fig. 3 shows the lasing spectra versus injection current before and after irradiation and demonstrates a jet color map plot of the spectrum as a function of the injection current. γ-ray radiation clearly does not affect the single-mode lasing characteristics of the laser. When the injection current exceeds 140 mA (twice the threshold current), the spectrum of the laser before and after irradiation maintains an SMSR of more than 60 dB. The higher SMSR comes from the apodized Bragg grating and its single longitudinal mode selection. Fig. 3 (b) and (d) also show that the laser has stable single-mode lasing characteristics in the full operating current range, and the minimal difference between the characteristics is only reflected in the injection current corresponding to the mode hopping position.

To further analyze the output power, SMSR and laser wavelength in the laser spectrum in detail, we created P–I–V characteristic curves of the laser before and after irradiation and curves for the SMSR and laser wavelength as a function of the injection current, as shown in Fig. 4.

The relationship between the output power and the injection current (Fig. 4 (a)) shows that the threshold current of the laser before and after irradiation is approximately 70 mA, and the slope efficiencies are 0.41 W/A and 0.43 W/A, respectively. The maximum output power increases from 137.23 mW before irradiation to 142.44 mW after irradiation. Radiation exposure caused slight changes in the laser power, and the reasons will be discussed below. Fig. 4 (b) and (c) show the influence of radiation corresponding to Fig. 3 on the SMSR and laser wavelength. The continuous wavelength tuning range of the laser before and after irradiation is approximately 31 p.m., which is basically consistent with the FSR of the equivalent resonator. The SMSRs of the laser before and after irradiation are 66.74 dB and 65.76 dB, and the corresponding laser wavelengths are 1030.0960 nm and 1030.1051 nm, respectively, at an injection current of 400 mA. The changes in the two are only 0.98 dB and 9.10 p.m., respectively. The impact of radiation on the SMSR and wavelength of the laser is weak.

The influence of γ-ray radiation on the wavelength and output power of the laser is mainly related to the generation of optical fiber defects induced by radiation. Radiation exposure is associated with the generation of defects, such as GeE′, Ge (1) and Ge (2) for Ge-doped fibers [23]. Defects will cause an increase in the effective refractive index of the fiber based on the Kramers-Kronig dispersion relationship. This will further cause a redshift of the Bragg resonance wavelength according to the phase matching condition of the Bragg grating. Because the laser wavelength is related to the Bragg resonance wavelength, the result will be a redshift of the laser wavelength. A. Morana et al. demonstrated that the wavelength change of a femtosecond-writing FBG after irradiation is approximately 10 p.m. [23]. The radiation-induced change in the laser wavelength in our work is consistent with the above report.

The reason for the radiation-induced change in the laser power is also related to the above radiation-induced defects. The generation of

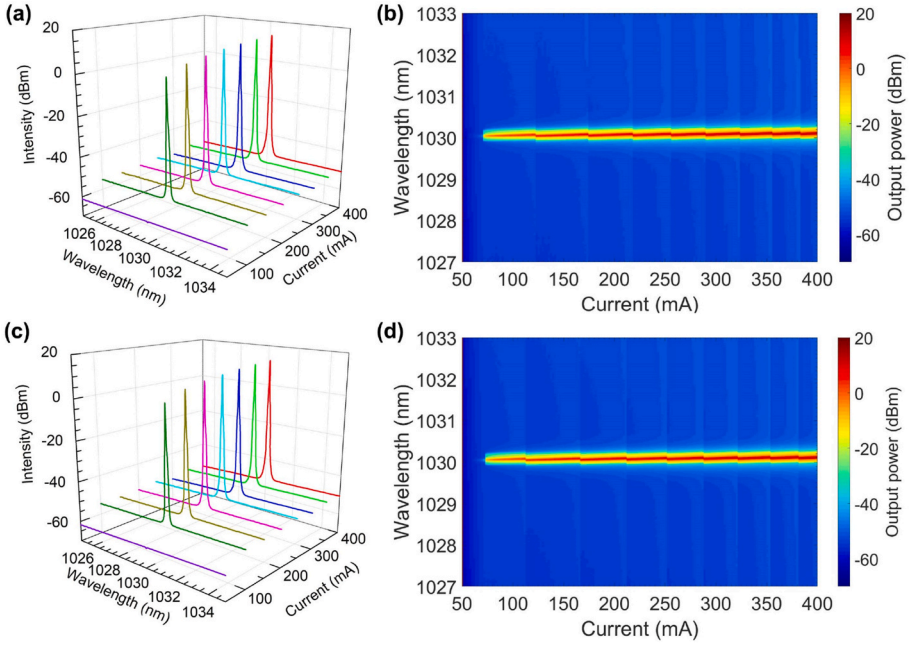

Fig. 3. Lasing spectra versus injection current: (a) spectra obtained using different currents and (b) jet map of the optical spectrum as a function of the injection current before irradiation; (c) spectra obtained using different currents and (d) jet map of the optical spectrum as a function of the injection current after irradiation.

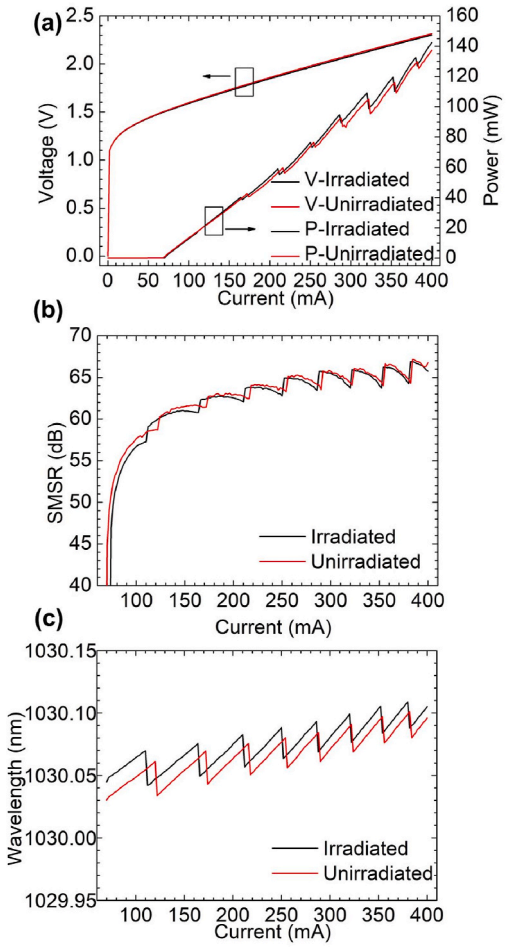

Fig. 4. (a) P–I–V curves of the laser, (b) SMSR versus injection current and (c) wavelength versus injection current before and after irradiation.

defects decreases the difference in the grating refractive index changes which decreases the refractive index modulation [18], thereby reducing the reflectivity of the Bragg grating. Because weak external optical feedback is conducive to an increase in output power, irradiation induces an increase in the laser power. To pursue absolute stability of the laser power in the application process in a specific space environment and avoid slight fluctuations in the power, the erasure of the type I refractive index modulation from the color center structure can be solved by high temperature or radiation pretreatment to strengthen the stability of the femtosecond FBG [20], and a small injection current can be adjusted to compensate for the weak impact of radiation accumulation. However, the influence of ray radiation on the photoelectric performance of the laser is weak from the analysis of the experimental results, and the developed laser shows significant radiation resistance.

3.2. Phase/frequency noise and linewidth characteristics

The linewidth characteristic is the key index of the laser, and we used the modified Schawlow-Townes equation to analyze the linewidth of the ECSL [32–34]. An external cavity laser can be considered a combination of an active gain region and a passive external cavity, and the Lorentz linewidth of the laser can be analyzed as follows:

$$\Delta\nu = \frac{\left(\Gamma v_g g_{th}\right)^2 \eta_0 h\nu n_{sp}\left(1+\frac{2}{H}\right)}{4\pi p}\left(\frac{n_{GC}L_{GC}}{n_{GC}L_{GC}+n_{ext}L_{ext}}\right)^2 \quad (1)$$

where Γ represents the constraint factor, v_g is the group velocity in the active region, g_{th} is the threshold gain, η_0 is the single-facet effectiency, $h\nu$ is the photon energy, n_{sp} is referred to as the spontaneous emission factor, α_H is the linewidth enhancement factor, and n_{GC} (n_{ext}) is the active (passive) region group index. The quality factor Q of the resonator is increased by expanding the cavity length of the resonator, while the photon life is extended and the intrinsic linewidth is suppressed. An increase in the output power is also helpful for achieving a narrower linewidth. The relationship between the output power and injection current must be established to analyze the change in the laser linewidth with output power. The output power of the ECSL can be expressed by the following equation:

$$P = \frac{I - I_{th}}{q\Gamma a v_g (N - N_0)} \tag{2}$$

where q represents the amount of charge, a represents the differential gain, N is the carrier density, and I_{th} represents the threshold current. The carrier density and photon number are enhanced with increasing injection current. The relationship between the theoretical Lorentz linewidth of the equivalent resonator and the injection current can be obtained based on the above equations, as shown by the solid line in Fig. 6.

Because the measurement range and accuracy of the traditional delayed self-heterodyne method are limited by the length of the delay optical fiber, we choose to derive and evaluate the linewidth in different Fourier frequency domains based on the β isolation line integration theory of the power spectral density (PSD), and we can understand how the frequency noise affects the change in the laser linetype. The single sideband PSD $L(f)$ of the phase noise and frequency noise PSD $S_{\delta v}(f)$ directly determine the frequency linewidth of the laser. The relationship between them can be determined by the following formula:

$$S_{\delta v}(f)\left[Hz^2/Hz\right] = 2f^2 L(f) \tag{3}$$

The laser linetype (Lorentz or Gaussian lines) can be determined by Fourier transform of the optical field autocorrelation function according to the Wiener–Khintchine theorem. The cutoff frequency f_c is defined as the intersection point between the β isolation line and the frequency noise PSD $S_{\delta v}(f)$; the frequency $f < f_c$ when the frequency noise is in the low-frequency stage. The linetype for this type of linewidth is a Gaussian distribution according to previous research [35,36], and the linewidth decreases with increasing frequency. The linewidth can be defined by integrating area A of the frequency noise component:

$$\Delta v_{\text{integral}} = \sqrt{8\,ln(2)A} \tag{4}$$

where the noise component area A is defined as follows:

$$A = \int_{\frac{1}{T_0}}^{\infty} \left[S_{\delta v}(f) - \frac{8\ln(2)f}{\pi^2}\right] S_{\delta v}(f)df \tag{5}$$

T_0 represents the measurement time corresponding to the cutoff frequency f_c, that is, $f_c = 1/T_0$. The white noise is the main contribution when $f > f_c$, and this laser linewidth is distributed according to the Lorentz type. The Lorentz linewidth can be determined by the white noise h_0:

$$\Delta v_{\text{Lorentz}} = \pi h_0 \tag{6}$$

The unbalanced Michelson interferometer for laser frequency noise measurement consists of 3 × 3 couplers and 2 F rotating mirrors (FRMs) [34,37]. Fig. 5 shows the phase noise power spectra (Fig. 5. (a) and (c)) of the laser before and after irradiation at 25 °C and 400 mA, and the corresponding frequency noise power spectra (Fig. 5 (b) and (d)) are

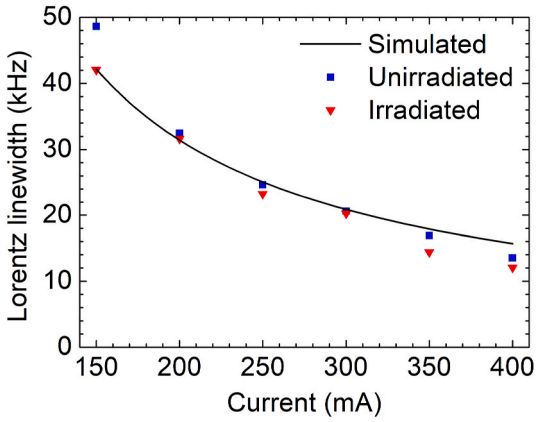

Fig. 6. Calculated and measured values of the Lorentz linewidth before and after irradiation.

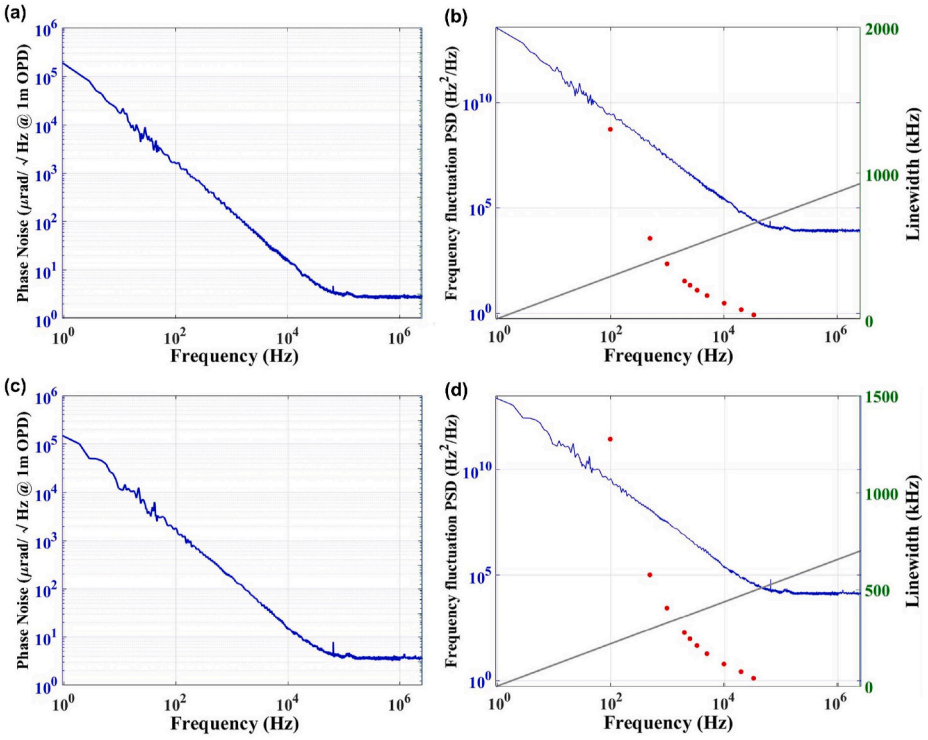

Fig. 5. (a) Phase noise power spectrum and (b) frequency noise power spectrum along with the linewidth before irradiation; (c) phase noise power spectrum and (c) frequency noise power spectrum along with the linewidth after irradiation.

obtained according to the above derived formula (3); the corresponding minimum integral linewidth and Lorentz linewidth are calculated. The minimum integral linewidth before irradiation is 25.60 kHz, and the white noise is 4300 Hz^2/Hz@2 MHz, which corresponds to a minimum Lorentz linewidth of 13.50 kHz. The minimum integrated linewidth and Lorentz linewidth after irradiation are 42.80 kHz and 12.00 kHz, respectively. The integral linewidth is obtained by integrating the component area A of the frequency noise PSD, which contains the Gaussian linetype component caused by the low-frequency noise, so the integral linewidth obtained is slightly larger than the Lorentz linewidth [38]. Fig. 6 shows the calculated and measured values of the Lorentz linewidth before and after irradiation. The measured linewidth is consistent with the calculated value. The output power correspondingly increases, and the linewidth gradually decreases as the injection current increases, which is consistent with the modified Schawlow–Townes equation. The Lorentz linewidths of the laser are almost the same before and after irradiation. The difference in the linewidth before and after irradiation may be due to errors in the test process.

3.3. Relative intensity noise characteristics

To evaluate the noise level of the laser, the RIN of the laser is tested. The test system mainly includes a photodiode, an RF amplifier and an electrical spectrum analyzer. Fig. 7 shows the RIN obtained using different currents before and after irradiation. The RIN of the laser before irradiation is −142.90 dBc/Hz@1 kHz and −153.80 dBc/Hz@1 MHz at 400 mA. The RIN after irradiation is −140.40 dBc/Hz@1 kHz and −154.20 dBc/Hz@1 MHz. RIN shows the characteristics of 1/f noise below 100 kHz and multiple peaks in the spectrum. This is due to the impact of technical noise during testing. The RIN tends to be stable above 100 kHz. The RIN power spectrum for the same current before and after irradiation fluctuates slightly, which is due to the carrier fluctuation caused by the mechanical noise in the connection device and the error in the test process. The fluctuation range of the RIN spectrum has almost no change after the laser passes through the γ-ray TID radiation, and the laser has excellent space environment adaptability.

4. Conclusions

In this work, we demonstrate a narrow-linewidth ECSL for radiation resistance that can be used in space laser communication. It is fabricated by coupling and integrating a permanent index modulated FBG with a QD gain chip. The laser shows very little change in performance after the TID radiation test using γ-rays. The maximum output power is only increased by 3.79%, the laser wavelength is redshifted by 9.10 p.m. and the variation in the SMSR is less than 0.98 dB compared with those before radiation. The minimum Lorentz linewidth and RIN of the laser are less than 15 kHz and −150 dBc/Hz, respectively, and they have almost no change after irradiation. The experimental results show that the compact-structure and low-cost laser have excellent reliability and robustness for space radiation environments and can be used in space laser communication.

Credit author statement

Jia-Qi Chen: Methodology, Investigation, Writing – original draft. **Chao Chen**: Conceptualization, Methodology, Validation, Writing – original draft, Writing – review & editing. **Qi Guo**: Formal analysis. **Li Qin**: Supervision. **Jian-Wei Zhang**: Data curation. **Hang-Yu Peng**: Visualization. **Jing-Jing Sun**: Formal analysis. **Xing Zhang**: Visualization. **Hao Wu**: Visualization. **Yin-Li Zhou**: Visualization. **Yong-Sen Yu**: Formal analysis. **Yong-Qiang Ning**: Project administration. **Li-Jun Wang**: Resources.

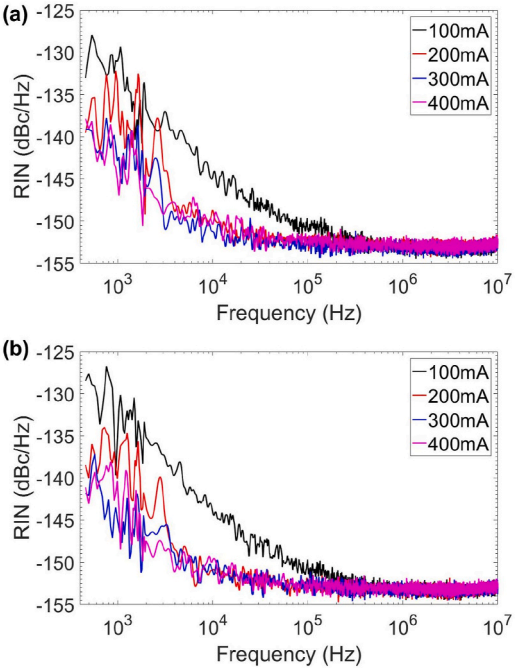

Fig. 7. RIN PSD of the laser obtained using different currents before (a) and after (b) irradiation.

Declaration of competing interest

The authors declare that they have no known competing financial interests or personal relationships that could have appeared to influence the work reported in this paper.

Data availability

Data will be made available on request.

Acknowledgements

This work is supported by the National Natural Science Foundation of China (61874119, 61727822, 11774343, 51672264), Science and Technology Development Project of Jilin Province (20220201063GX, 20200401006GX), Changchun Science and Technology Development Plan Project (22SH01), and Finance Science and Technology Project of Hainan Province (ZDYF2020217).

References

[1] Z. Sodnik, B. Furch, H. Lutz, Optical intersatellite communication, IEEE J. Sel. Top. Quant. Electron. 1 (2010) 1051.
[2] S. Girard, A. Laurent, E. Pinsard, T. Robin, B. Cadier, M. Boutillier, C. Marcandella, A. Boukenter, Y. Ouerdane, Radiation-hard erbium optical fiber and fiber amplifier for both low- and high-dose space missions, Opt. Lett. 39 (9) (2014) 2541–2544.
[3] H. Christopher, B. Arar, A. Bawamia, C. Kürbis, W.L. Adamczyk, M. Schiemangk, R. Smol, A. Wicht, A. Peters, G. Tränkle, Narrow Linewidth Micro-integrated High Power Diode Laser Module for Deployment in Space, IEEE. ICSOS, 2017, pp. 150–153.
[4] C. Kürbis, A. Bawamia, M. Krüger, R. Smol, A. Peters, A. Wicht, G. Tränkle, Extended cavity diode laser master-oscillator-power-amplifier for operation of an iodine frequency reference on a sounding rocket, Appl. Opt. 59 (2) (2020) 253–262.
[5] A. Bawamia, C. Kuerbisa, R. Smola, A. Wichta, Semiconductor Laser Modules for Precision Spectroscopy Applications in Space, Proc. SPIE, 2018, p. 111805C.
[6] S. Spießberger, M. Schiemangk, A. Sahm, A. Wicht, H. Wenzel, A. Peters, G. Erbert, G. Trankle, Micro-integrated 1 watt semiconductor laser system with a linewidth of 3.6 kHz, Opt Express 19 (8) (2011) 7077–7083.
[7] K. Dahl, P. Cebecib, O. Fitzaub, M. Giesbertsb, C. Grevef, M. Krutzikd, A. Petersd, S. A. Pykad, J. Sanjuane, M. Schiemangkc, T. Schuldte, K. Vossa, A. Wichtc, A New Laser Technology for LISA, Proc. SPIE, 2018, p. 111800C.

[8] M. Schiemangk, A. Wichta, G. Tränklea, Ultra-narrow Linewidth Diode Laser Based on Resonant Optical Feedback, Proc. SPIE, 2019, p. 109101U.
[9] L. Duca, E. Perego, F. Berto, C. Sias, Design of a littrow-type diode laser with independent control of cavity length and grating rotation, Opt. Lett. 46 (12) (2021) 2840–2843.
[10] D. Shin, B. Henson, R. Khakimov, J. Ross, C. Dedman, S. Hodgman, K. Baldwin, A. Truscott, Widely tunable, narrow linewidth external-cavity gain chip laser for spectroscopy between 1.0-1.1 μm, Opt Express 24 (24) (2016) 27403–27414.
[11] Y. Shi, S. Li, Y. Zhou, L. Lu, L. Li, Y. Feng, X. Chen, Improved λ/4 phase-shifted DFB semiconductor laser with spatial hole burning compensation using grating chirp, Opt Laser. Technol. 44 (2012) 2443–2448.
[12] Y. Hai, Y. Zou, X. Ma, J. Fan, H. Wang, L. Zhu, L. Shi, Narrow-linewidth surface-emitting distributed feedback semiconductor lasers with low threshold current, Opt Laser. Technol. 135 (2021), 106631.
[13] K. Numata, M. Alalusi, L. Stolpner, G. Margaritis, J. Camp, M. Krainak, Characteristics of the single-longitudinal-mode planar-waveguide external cavity diode laser at 1064 nm, Opt. Lett. 39 (7) (2014) 2101–2104.
[14] Y. Zhu, L. Zhu, Narrow-linewidth, tunable external cavity dual-band diode lasers through InP/GaAsSi_3N_4 hybrid integration, Opt Express 27 (3) (2019) 2354–2362.
[15] A.P. Bakoz, A.A. Liles, A.A. Gonzalez-Fernandez, T. Habruseva, C. Hu, E. A. Viktorov, S.P. Hegarty, L. O'Faolain, Wavelength stability in a hybrid photonic crystal laser through controlled nonlinear absorptive heating in the reflector, Light Sci. Appl. 7 (2018) 39.
[16] M. Lancry, B. Poumellec, UV laser processing and multiphoton absorption processes in optical telecommunication fiber materials, Phys. Rep. 523 (4) (2013) 207–229.
[17] A. Morana, S. Girard, E. Marin, M. Lancry, J. Grelin, C. Marcandella, P. Paillet, A. Boukenter, Y. Ouerdane, Dependence of the voids-fiber Bragg grating radiation response on temperature, dose, and dose rate, IEEE Trans. Nucl. Sci. 65 (8) (2018) 1619–1623.
[18] A. Morana, S. Girard, E. Marin, C. Marcandella, P. Paillet, J. Périsse, J.R. Macé, A. Boukenter, M. Cannas, Y. Ouerdane, Radiation tolerant fiber Bragg gratings for high temperature monitoring at MGy dose levels, Opt. Lett. 39 (118) (2014) 5313–5316.
[19] A. Gusarov, B. Brichard, D. Nikogosyan, Gamma-radiation effects on Bragg gratings written by femtosecond UV laser in Ge-doped fibers, IEEE Trans. Nucl. Sci. 57 (4) (2010) 2024–2028.
[20] A. Morana, S. Girard, E. Marin, M. Lancry, C. Marcandella, P. Paillet, L. Lablonde, T. Robin, R.J. Williams, M.J. Withford, A. Boukenter, Y. Ouerdane, Influence of photo-inscription conditions on the radiation-response of fiber Bragg gratings, Opt Express 23 (7) (2015) 8659–8669.
[21] S. Qiao, P. Ma, V. Tsepelin, G. Han, J. Liang, W. Ren, H. Zheng, Y. Ma, Super tiny quartz-tuning-fork-based light-induced thermoelastic spectroscopy sensing, Opt. Lett. 48 (2) (2023) 419–422.
[22] Y. Liu, Y. Ma, Advances in multipass cell for absorption spectroscopy-based trace gas sensing technology [Invited], Chin. Opt Lett. 21 (3) (2023), 033001.
[23] X. Liu, Y. Ma, Sensitive carbon monoxide detection based on light-induced thermoelastic spectroscopy with a fiber-coupled multipass cell [Invited], Chin. Opt Lett. 20 (3) (2022), 031201.
[24] D. Sporea, A. Sporeaa, I. Vatab, Comparative Study of Gamma-Ray and Neutron Irradiated Laser Diodes, Proc. SPIE, 2007, p. 67962R.
[25] Y. Zhou, J. Zhang, Y. Ning, Y. Zeng, J. Zhang, X. Zhang, L. Qin, L. Wang, Bimodal-sized quantum dots for broad spectral bandwidth emitter, Opt Express 23 (25) (2015) 32230–32237.
[26] J.W. Mares, J. Harben, A.V. Thompson, D.W. Schoenfeld, W.V. Schoenfeld, Gamma radiation induced degradation of operating quantum dot lasers, IEEE Trans. Nucl. Sci. 55 (2) (2008) 763–768.
[27] R.J. Williams, R.G. Kramer, S. Nolte, M.J. Withford, M.J. Steel, Detuning in apodized point-by-point fiber Bragg gratings: insights into the grating morphology, Opt Express 21 (22) (2013) 26854–26867.
[28] Q. Guo, Z. Zheng, B. Wang, X. Pan, S. Liu, Z. Tian, C. Chen, Y. Yu, Femtosecond laser fabricated apodized fiber Bragg gratings based on energy regulation, Photonics 8 (2021) 110.
[29] B. Timmons, R.E. Stoner, Radiation exposure of distributed-feedback lasers for use in atom trapping and atom interferometry, IEEE Trans. Nucl. Sci. 58 (2) (2011) 490–498.
[30] H. Henschel, S.K. Hoeffgen, J. Kuhnhenn, U. Weinand, Influence of manufacturing parameters and temperature on the radiation sensitivity of fiber Bragg gratings, IEEE Trans. Nucl. Sci. 57 (4) (2010) 2029–2034.
[31] H. Henschel, D. Grobnic, S.K. Hoeffgen, J. Kuhnhenn, S.J. Mihailov, U. Weinand, Development of highly radiation resistant fiber Bragg gratings, IEEE Trans. Nucl. Sci. 58 (4) (2011) 2103–2110.
[32] C. Henry, Theory of the linewidth of semiconductor lasers, IEEE J. Quant. Electron. 18 (1982) 259–264.
[33] L.A. Coldren, S.W. Corzine, Diode Lasers and Photonic Integrated Circuits, vol. 5, John Wiley & Sons, Inc., New York, 2012, pp. 303–328.
[34] X. Luo, C. Chen, Y. Ning, J. Zhang, J. Chen, X. Zhang, L. Li, H. Wu, Y. Zhou, L. Qin, L. Wang, Single polarization, narrow linewidth hybrid laser based on selective polarization mode feedback, Opt Laser. Technol. 154 (2022), 108340.
[35] L. Tombez, S. Schilt, J.D. Francesco, T. Führer, B. Rein, T. Walther, G.D. Domenico, D. Hofstetter, P. Thomann, Linewidth of a quantum-cascade laser assessed from its frequency noise spectrum and impact of the current driver, Appl. Phys. B 109 (2012) 407–414.
[36] N. Bucalovic, V. Dolgovskiy, C. Schori, P. Thomann, G. Domenico, S. Schilt, Experimental validation of a simple approximation to determine the linewidth of a laser from its frequency noise spectrum, Appl. Opt. 51 (20) (2012) 4582–4588.
[37] Q. Zhou, J. Qin, W. Xie, Z. Liu, Y. Tong, Y. Dong, W. Hu, Power-area method to precisely estimate laser linewidth from its frequency-noise spectrum, Appl. Opt. 54 (28) (2015) 8282–8289.
[38] N.V. Bandel, M. Myara, M. Sellahi, T. Souici, R. Dardaillon, P. Signoret, Time-dependent laser linewidth: beat-note digital acquisition and numerical analysis, Opt Express 24 (24) (2016) 27961–27978.